Available online at www.sciencedirect.com
ScienceDirect
Journal of Solid State Chemistry 180 (2007) 1672–1677
JOURNAL OF SOLID STATE CHEMISTRY
www.elsevier.com/locate/jssc

Structure and physical properties of BaCuTeF

Cheol-Hee Park[a], Robert Kykyneshi[b], Alexandre Yokochi[c], Janet Tate[b], Douglas A. Keszler[a,*]

[a]Department of Chemistry, 153 Gilbert Hall, Oregon State University, Corvallis, OR 97331-4003, USA
[b]Department of Physics, 301 Weniger Hall, Oregon State University, Corvallis, OR 97331-6507, USA
[c]Department of Chemical Engineering, 102 Gleeson Hall, Oregon State University, Corvallis, OR 97331-2702, USA

Received 8 January 2007; received in revised form 21 March 2007; accepted 26 March 2007
Available online 28 March 2007

Abstract

The compound BaCuTeF has been prepared by using high-temperature reaction methods, and its structure has been established via Rietveld refinement of powder X-ray diffraction data. It crystallizes in the tetragonal space group $P4/nmm$ (No. 129) with $Z = 2$, $a = 4.4297\,(1)$, $c = 9.3706\,(1)$ Å, and $V = 183.87\,(1)$ Å^3; refinement residuals include $R_p/wR_p/R_{Bragg}$ (%) = 6.72/4.42/5.72. A band gap of 2.3 eV is estimated from wavelength-dependent diffuse reflectance measurements. Room-temperature conductivities of pressed pellets are 6–8 S/cm, and variable-temperature Seebeck and electrical-conductivity measurements reveal *p*-type degenerate semiconductor behavior.

Keywords: BaCuTeF; Rietveld refinement; *p*-type degenerate semiconductor

1. Introduction

The materials MCuQF (M = Ba, Sr; Q = S, Se, Te) exhibit a unique combination of *p*-type conductivity and band gaps that allow transmission of much of the visible spectrum [1,2]. BaCuSF, for example, is transparent in thin-film form throughout the visible with a measured band gap as high as 3.2 eV [3]. The room-temperature Seebeck coefficients and electrical conductivities of undoped BaCuSF pellets have been determined to be +56 μV/K and 0.09 S/cm, respectively. The conductivity can be considerably enhanced by substitution of K for Ba with the highest value of 82 S/cm found for the composition $Ba_{0.9}K_{0.1}CuSF$ [4]. The material exhibits strong, saturated red luminescence near 630 nm following band-gap excitation, and a gradual change in emission color to saturated green is observed on modification of the synthesis conditions and by selective doping [2].

In a previous contribution, band-gap modulation was demonstrated by changing Q in the solid-solution series $BaCuS_{1-x}Se_xF$ and $BaCuSe_{1-y}Te_yF$ ($0 \leqslant x \leqslant 1$; $0 \leqslant y \leqslant 0.5$) [1]. The gaps across these series were tuned from 3.2 to 2.9 eV by substitution of Se for S and then to 2.7 eV by partial substitution of Te for Se ($y = 0.5$). The decrease in band gap on substitution of the heavier Group 16 congeners for S is partially derived from the increased size of Q and the consequent increase in band dispersion; the fall in band gap also scales in a nearly linear manner with respect to the increase in unit-cell volume. From local density approximation band-structure calculations and photoemission experiments [5], the top of the valence band in BaCuQ$F was found to be mainly composed of a mixture of Cu 3*d* and Q *np* orbitals. Typically, higher covalency will give broader bands and smaller effective masses, which give rise to higher carrier mobilities [6]. Therefore, strong Cu–Te orbital mixing in BaCuTeF should afford higher mobility and electrical conductivity relative to the other members of the BaCuQ$F family. Extrapolation of previous data on band gaps in the series $BaCuSe_{1-x}Te_xF$ also indicate that the gap of BaCuTeF should fall in a region of interest for use as a transparent back contact in wide-gap thin-film photovoltaic cells.

In our previous work on the series $BaCuSe_{1-y}Te_yF$, experiments were limited to $y_{max} = 0.5$ by our inability to acquire or synthesize BaTe, which is a key reagent for the

*Corresponding author. Fax: +1 541 737 2062.
E-mail address: douglas.keszler@oregonstate.edu (D.A. Keszler).

0022-4596/$ - see front matter © 2007 Elsevier Inc. All rights reserved.
doi:10.1016/j.jssc.2007.03.021

synthesis of samples having a Te fraction $y > 0.5$. We have now prepared BaTe, and we report here the successful synthesis of BaCuTeF, its refined structure, transport and optical properties, and results of band-structure calculations. Its room-temperature conductivity is much higher than those of undoped BaCuSF and BaCuSeF, and the temperature dependencies of its electrical conductivity and Seebeck coefficient are consistent with *p*-type degenerate semiconductor behavior.

2. Experimental

2.1. Synthesis

Reagents for synthesis of BaCuTeF were BaTe (synthetic details given below), Cu_2Te (Cerac, 99.5%), and BaF_2 (Cerac, 99.9%). The constituent materials were intimately mixed in stoichiometric proportions and heated in an evacuated silica tube at 500 °C for 12 h. Product characterization by powder X-ray diffraction analysis revealed a mixture of the desired phase and BaF_2. The sample was subsequently annealed with a 5 wt% excess of Te (Alfa, 99.9%) at 500 °C under flowing H_2(5%)/N_2(95%).

BaTe was prepared by using Ba metal (Alfa, 99.2% in oil) and Te. After carefully washing the Ba several times with *n*-hexane, while preventing exposure to air, it was introduced into an Ar-filled glove box. The white oxide surface on the metal was removed with a scalpel, and the resulting material was placed in a silica tube with a stoichiometric amount of Te. The silica tube was evacuated, sealed, and heated at 575 °C for 5 h. The powder X-ray diffraction pattern of the product matched that reported for BaTe [7].

2.2. Structural characterization

Data for the Rietveld structural refinement were collected on a 1:1 mixture by weight of BaCuTeF and LiF by using a Siemens D5000 diffractometer with variable slits and a locally devised variable counting-time routine [8]. Data were converted to GSAS ESD format by using an in-house program, and structural refinement was performed by using the program Fullprof [9].

During refinement, analysis revealed an anisotropic *hkl*-dependent line broadening associated with strain in the sample. In an effort to optimize the fit, the four possible parameters in Stephen's formalism [10] of strain broadening for this Laue class were refined, resulting in substantial improvements in residuals. In the program Fullprof, an integral breadth contribution from strain (β_{str}) with units of 10^{-4} Å^{-1} is calculated from the refined parameters with $S_{hkl} = \frac{1}{2} * \beta_{str} * d_{hkl}$. The value thus obtained is approximately equivalent to $\frac{1}{4}$ of the value of the equivalent Stokes–Wilson apparent strain. Final crystallographic parameters for this refinement, including calculated strain parameters, are given in Table 1, and positional parameters and equivalent isotropic displacement parameters are listed in Table 2.

Table 1
Summary of collection and refinement data for BaCuTeF

Formula	BaCuTeF
Space group	*P*4/*nmm* (no. 129)
Z	2
a (Å)	4.4297(1)
c (Å)	9.3706(1)
Vol (Å^3)	183.87(1)
Fw (amu)	347.94
Calculated density (g/cm^3)	6.279
2θ range (deg.)	10.0–150.0
2θ step (deg.)	0.02
Profile points	7001
S_{400}	0.37(2)
S_{004}	0.067(4)
S_{220}	1.01(10)
S_{202}	0.00(2)
Calculated strain (10^{-4}) in given crystallographic direction	
100	7.52
101	6.24
111	7.22
110	8.13
001	14.40
R_p (%)	6.72
R_{wp} (%)	4.42
R_{Bragg} (%)	5.72
Number of reflections	280
Number of parameters	13 Le Bail + 10 Rietveld

Table 2
Final positional and isotropic equivalent displacement parameters (Å$^2 \times 100$) for BaCuTeF

	Wyckoff	*x*	*y*	*z*	U_{iso}
Ba	2c	1/4	1/4	0.3443(2)	2.51(10)
Cu	2a	3/4	1/4	0	4.19(19)
Te	2c	1/4	1/4	−0.1636(2)	2.32(10)
F	2b	3/4	1/4	1/2	1.9(4)

2.3. Transport and optical property measurements

For transport property measurements, powder samples were pressed into 9.5-mm diameter pellets at 3 tons and annealed at 750 °C for 5 h in evacuated silica tubes. The conductivities of the pellets were measured by the four-probe collinear method over the temperature range 10–300 K. Seebeck measurements were made to establish the carrier sign by using a temperature gradient of 3 K over the temperature range 50–290 K.

The diffuse reflectance at room temperature of powder samples was measured with $BaSO_4$ as a reference and an optical setup comprised of an Oriel 300-W Xe lamp, a Cary model-15 prism monochromator, and a Hamamatsu

R636-10 photomultiplier tube, providing coverage of the UV–visible region (360–700 nm).

2.4. Band structure

The electronic structure of BaCuTeF was computed with the code Wien2k [11] in the full-potential linearized augmented plane-wave formalism with the PBE generalized gradient approximation. The crystal-structure parameters were those from the refined X-ray data, cf. Table 1. The muffin-tin radii were set to 2.5 au for Ba, Cu and F, and to 2.35 for Te. The potentials and charge densities were expanded on a k-mesh of 2500 points, including 180 unique k-points. Inside the spheres, these quantities were expanded up to $l = 10$. In the interstitial region, they were expanded by using 4183 plane waves. The calculations were iterated until the total energies converged to better than 0.1 mRy and total charge to better than $10^{-3}e$. No significant numerical errors in the band structure are observed in the resulting plots.

3. Results and discussion

The results of the final Rietveld refinement cycle are depicted in Fig. 1. The difference pattern and small residuals, cf., Table 1, are indicative of good agreement between the model and data. The compound BaCuTeF is isostructural to the materials BaCuQF (Q = S, Se) [1] and the oxide chalcogenides MCuOX (M = lanthanide, Bi; X = S, Se, Te) [12]. The structure is a layered, tetragonal type with antifluorite [Ba_2F_2] layers alternating with [Cu_2Te_2] sheets along the c-axis (Fig. 2).

The Ba and Te atoms occupy sites with symmetry C_{4v}. The Ba atom occupies a square antiprismatic environment with four Te atoms forming one square face and four F atoms the other. Selected interatomic distances are given in Table 3. The Ba–Te distance, 3.560(1) Å, compares well to those found in compounds such as $BaGa_2Te_4$ (3.562 Å) [13] and $BaAl_2Te_4$ (3.581 Å) [13]. The Ba–F distance, 2.652(1) Å, is similar to those observed in BaCuSF (2.613(1) Å), BaCuSeF (2.622(1) Å), and BaF_2 (2.684 Å) [2]. The Te atom is also located in a square antiprismatic site coordinated by four Ba atoms and four Cu atoms. The Cu and F atoms are located on sites having D_{2d} symmetry, representing distorted tetrahedral environments. The Cu atom, coordinated to four Te atoms, has a Cu–Te interatomic distance of 2.694(1) Å, which is comparable to the sum of covalent radii, 2.65 Å [14], and similar interactions in other tellurides such as NaCuTe (2.704 Å) [15] and $BaCu_2Te_2$ (mean = 2.673 Å) [16]. As evident from the Te–Cu–Te angles, cf. Table 3, the $CuTe_4$ unit is only slightly distorted from T_d symmetry.

The two-dimensional [Cu_2Te_2] tetragonal sheet structure has also previously been observed in NaCuTe [15]. These sheets are characterized by edge-sharing linkages of the distorted $CuTe_4$ tetrahedra, which produce relatively short Cu···Cu distances. The shortest Cu···Cu distance in

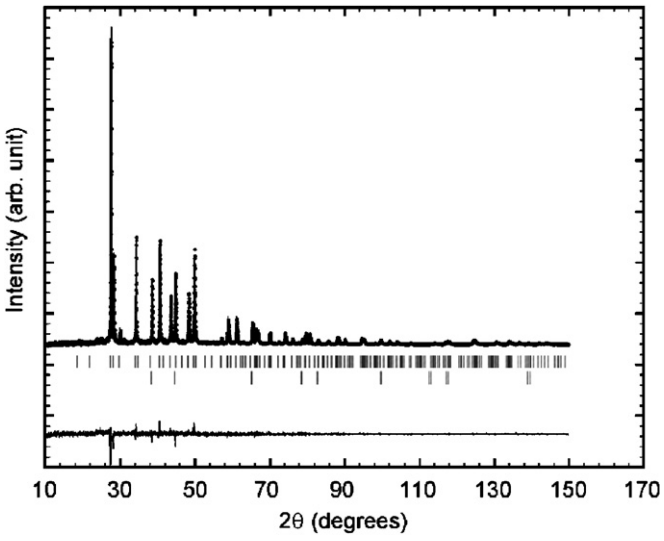

Fig. 1. Observed (open circles) and calculated (solid line) X-ray powder diffraction patterns from refinement of BaCuTeF. The bottom curve is the difference pattern on the same scale. The top vertical bars are for BaCuTeF and the lower vertical bars are for LiF.

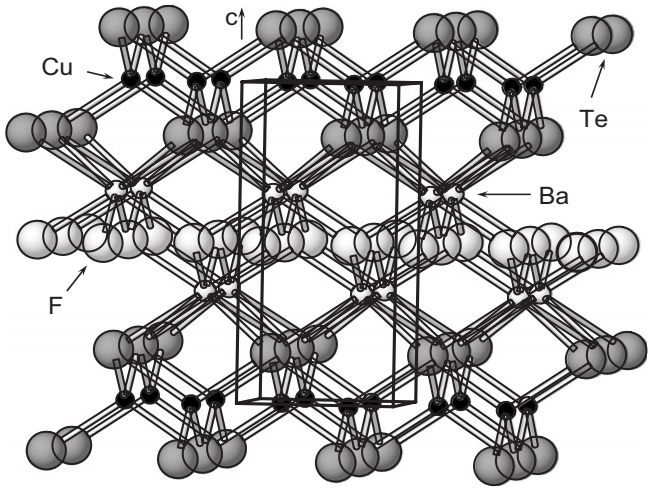

Fig. 2. Crystal structure of BaCuTeF.

Table 3
Selected interatomic distances (Å) and angles (deg.) for BaCuTeF

Cu–Te	2.694(1)	Te–Cu–Te	108.90(8)
Cu···Cu	3.1321(1)	Te–Cu–Te	110.61(4)
Ba–Te	3.560(1)	Te–Ba–Te	76.94(3)
Ba–F	2.652(1)	Te–Ba–Te	123.22(3)
Ba···Ba	4.281(2)	F–Ba–F	72.38(4)
		F–Ba–F	113.23(4)
		Te–Ba–F	75.06(5)
		Te–Ba–F	141.36(5)

The telluride fluoride BaCuTeF has been synthesized and structurally characterized through Rietveld refinement of X-ray diffraction data. It crystallizes in the tetragonal structure of LaCuOS. Optical and transport measurements have been used to establish the material as a degenerate p-type semiconductor with a band gap near 2.3 eV.

BaCuTeF is 3.1321(1) Å, which is comparable to that, 3.097 Å, observed in NaCuTe, but longer than the 2.847 Å observed in $BaCu_2Te_2$. A similar situation is found from comparison of Cu···Cu distances in BaCuSF (2.915 Å) and α-$BaCu_2S_2$ (2.71 Å), where CuS_4 tetrahedra also share edges. The longer Cu···Cu distance for BaCuTeF in comparison to that of $BaCu_2Te_2$ derives from the Te–Cu–Te angle associated with the shared Te···Te edge; these angles are 108.90(8)° for BaCuTeF and 115.8(1)° for $BaCu_2Te_2$. The larger angle forces a shorter Cu···Cu separation. Likewise, the S–Cu–S angle associated with the shortest Cu···Cu distance is 107.2° for BaCuSF and 112.8(2)° for α-$BaCu_2S_2$.

A bimodal distribution is observed in the anisotropic strain broadening parameters, cf. Table 1, i.e., strain in the *ab* plane is smaller than that along the *c*-axis. A small number of stacking faults likely occur in the material, which leads to preferential broadening of reflections with scattering vectors close to the *c* direction. Strain is also observed within the *ab* layers because of slight *ab* plane lattice mismatches associated with the *c*-axis stacking faults.

The absorption spectrum of powdered BaCuTeF, which was obtained from the diffuse reflectance spectrum by using the Kubelka–Munk method [17,18], is shown in Fig. 3. The absorption coefficient (α) increases moderately with increasing photon energy below approximately 2.2 eV. Between 2.2 and 2.8 eV, a steady increase is observed, and at an energy higher than approximately 2.9 eV, it is nearly constant. A band-gap energy of 2.3 eV was extracted by extrapolating the straight-line portion of the curve of $(\alpha E)^2$ vs. E to the abscissa (inset in Fig. 3). Because of the isolation of the two-dimensional $[Cu_2Te_2]$ sheets and the effects of quantum confinement, the observed band gap is considerably larger than that (1.1 eV) of the related three-dimensional solid Cu_2Te [19]. Also, as expected, it is smaller than the gaps of BaCuSeF (2.9 eV) and BaCuSF (3.2 eV). The overall unit-cell volume increase is 7% from BaCuSF to BaCuSeF and 12% from BaCuSeF to BaCuTeF. The decrease in band-gap energy in the series S→Se→Te is correlated to these cell-volume changes, reflecting the larger radial extension of the orbitals for the heavier congeners, which contribute to larger band widths both through Cu–Q and Q···Q interactions. From the plot, cf. Fig. 3, the material appears to have a direct band gap. We note, however, that the significant wavelength dispersion of the absorption edge is likely reflective of considerable defects and attendant mid-gap states in the powders. As noted in the discussion of the X-ray data, the powders do exhibit anisotropic strain likely associated with stacking faults along the *c*-axis.

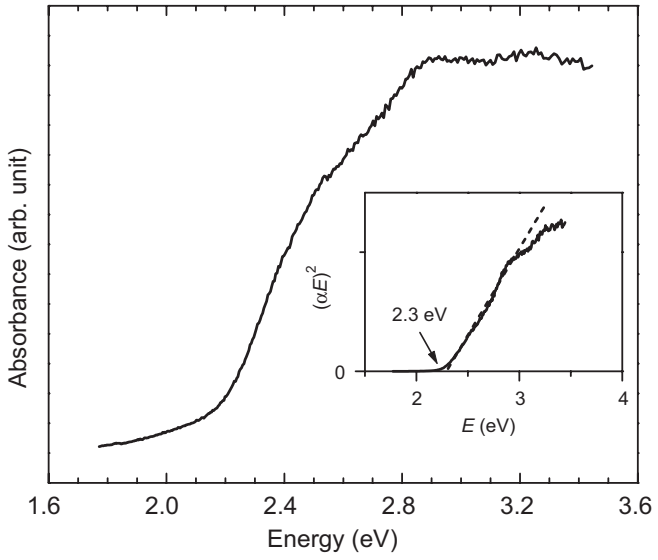

Fig. 3. Absorption spectrum of BaCuTeF at room temperature with the curve of $(\alpha E)^2$ vs. E (inset).

The main features of the band-structure calculation are illustrated in Figs. 4 and 5. Dispersion is greatest along high symmetry directions correlated to the *ab* plane of the crystal structure, reflecting the independence of the $[Cu_2Te_2]$ layers along the *c*-axis. The valence-band maximum and the conduction-band minimum are both located at the Γ point—consistent with a direct band gap. In this respect, BaCuTeF exhibits behavior similar to BaCuSeF and BaCuSF and a marked difference from the series LaCuOQ, where there is an indication of a changeover from the direct gaps of the S and Se members to an indirect gap for the Te member [20]. The total and partial densities of states in the region of the band gap are illustrated in Fig. 5. The main contributions to the valence band are Cu 3*d* and Te 5*p* orbitals, being antibonding in character. The conduction band minimum is primarily Cu 4*s* in character with Te orbitals mixing more strongly slightly above the minimum. On the basis of similar calculations, the conduction band of BaCuTeF is notably more disperse than that of either BaCuSeF or BaCuSF. If *n*-type doping were possible, relatively high mobility could result.

Undoped BaCuTeF exhibits a modest increase in conductivity with decreasing temperature (Fig. 6), indicating the metal-like behavior of a degenerate semiconductor. This conductivity contrasts to the activated semiconducting behavior of undoped BaCuSF and the intermediate

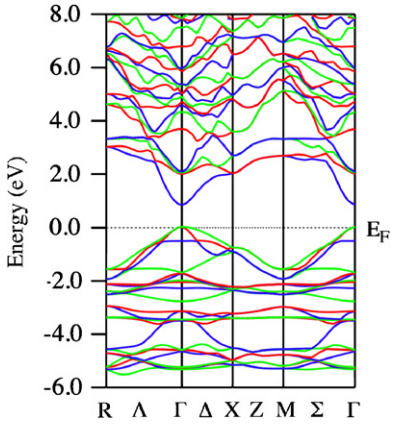

Fig. 4. Band stucture of BaCuTeF.

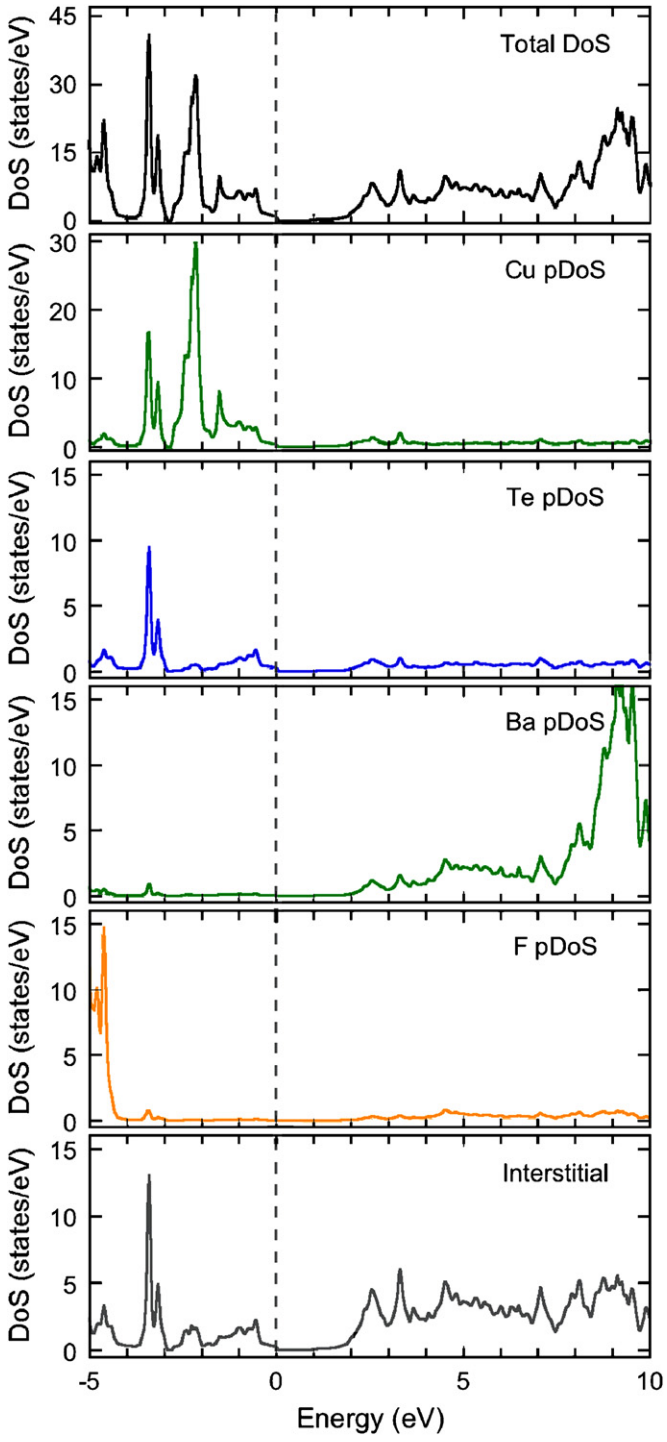

Fig. 5. Density of states for BaCuTeF. The Fermi energy is set to zero at the top of the valence band. Note: the Cu partial density of states is scaled by a factor of 2 relative to the others, and the total density of states by a factor of 3.

behavior of BaCuSeF (inset Fig. 6) [3]. The latter two compounds exhibit metal-like behavior only after *p*-type doping with K substitution for Ba. A similar change from semiconducting to degenerate behavior is also observed in the orthorhombic series $BaCu_2Q_2$ (Q = S, Se, Te); orthorhombic $BaCu_2S_2$ and $BaCu_2Se_2$ exhibit activated semiconducting behavior, whereas $BaCu_2Te_2$ exhibits a metallic temperature dependence in conductivity [2,16].

The room temperature conductivities of BaCuTeF pellets are measured as 6–8 S/cm, two orders of magnitude higher than those of undoped BaCuSF (0.09 S/cm) and BaCuSeF (0.08 S/cm). It should be noted that the room-temperature conductivity of $BaCu_2S_2$ sintered pellets is also two orders of magnitude lower than that of $BaCu_2Te_2$ pellets [2,16]. The lower room temperature conductivity of BaCuTeF in comparison to that of powdered $BaCu_2Te_2$ (127 S/cm) could be in part attributed to the longer Cu···Cu distance. Another contribution may be found in the differing linkages of the $CuTe_4$ tetrahedra. In BaCuTeF, $CuTe_4$ tetrahedra are connected in only two dimensions, in contrast to the three-dimensional linkage of $CuTe_4$ tetrahedra in $BaCu_2Te_2$. The dimensional reduction in BaCuTeF should lead to an anisotropic conductivity, which in a pressed pellet could produce an underestimation of the conductivity in the $[Cu_2Te_2]$ sheets.

Measurements of the Seebeck coefficient, falling in the range of +25 to +55 μV/K, confirm the positive sign of the carriers at room temperature. As expected for a material whose carriers are induced by unintentional doping, the measured values are highly dependent on the details of the preparation. All measurements have

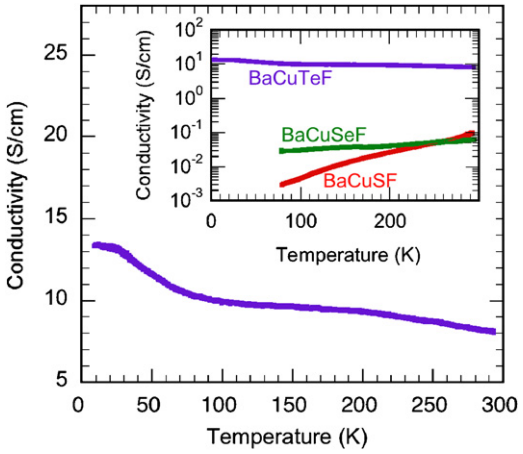

Fig. 6. The conductivity of BaCuTeF (main graph) increases with decreasing temperature, in contrast to that of BaCuSF and BaCuSeF (inset).

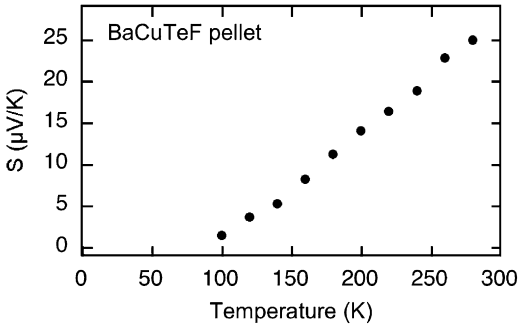

Fig. 7. Temperature dependence of Seebeck coefficient of BaCuTeF.

produced positive signs covering a relatively narrow range in magnitude. The Seebeck coefficient for undoped BaCuTeF increases with increasing temperature (Fig. 7), and it is approximately linear from 100 to 290 K, also indicating metal-like behavior.

Chalcogenides of Cu are well-known *p*-type semiconductors. A propensity for Cu-vacancy formation and extensive Cu–*Q* orbital mixing readily lead to hole formation and *p*-type conductivity. BaCuTeF is a new member of this broad Cu–chalcogenide family. In the current powder form, as described here, the material contains numerous defects most likely dominated by a high Cu-vacancy concentration. Improvements in preparative schemes should yield products exhibiting higher band gaps, hole mobilities, and conductivities. Indeed, our recent efforts in thin-film growth to be described in forthcoming contributions have produced such results.

4. Conclusion

A new member of the BaCu*Q*F family, BaCuTeF, has been prepared by high-temperature reaction methods, and its structure has been refined via the Rietveld refinement method of powder diffraction data. Its band gap is estimated to be 2.3 eV from wavelength-dependent diffuse reflectance measurements, and temperature-dependent Seebeck coefficient and conductivity measurements clearly indicate that it is a *p*-type degenerate semiconductor.

Acknowledgments

This material is based on work supported by the Department of Energy through the National Renewable Energy Laboratory (Subcontract no. XAT-4-33624-11 to DAK) and by the National Science Foundation (Grant no. DMR-0245386 to JT).

References

[1] C.-H. Park, D.A. Keszler, H. Yanagi, J. Tate, Thin Solid Films 445 (2003) 288.
[2] C.-H. Park, Ph.D. Dissertation, Oregon State University, 2005.
[3] H. Yanagi, S. Park, A.D. Draeseke, D.A. Keszler, J. Tate, J. Solid State Chem. 175 (2003) 34.
[4] H. Yanagi, J. Tate, S. Park, C.-H. Park, D.A. Keszler, Appl. Phys. Lett. 82 (2003) 2814.
[5] H. Yanagi, J. Tate, D.A. Keszler, S. Park, C.-H. Park, H. Masahiro, H. Hosono, J. Appl. Phys. 100 (2006) 083705/1.
[6] P.A. Cox, The Electronic Structure and Chemistry of Solids, Oxford University Press, Oxford, 1987.
[7] JCPDS # 39-1475.
[8] I.C. Madsen, R.J. Hill, J. Appl. Crystallogr. 27 (1994) 385.
[9] J. Rodriguez-Carvajal, Physica B 192 (1993) 55.
[10] P. Stephens, J. Appl. Crystallogr. 32 (1999) 281.
[11] P. Blaha, K. Schwarz, G. K. H. Madsen, D. Kvasnicka, J. Luitz, WIEN2k, An Augmented Plane Wave + Local Orbitals Program for Calculating Crystal Properties, Karlheinz Schwarz, Technical Universität, Wien, Austria, 2001.
[12] P.S. Berdonosov, A.M. Kusainova, L.N. Kholodkovskaya, V.A. Dolgikh, L.G. Akselrud, B.A. Popovkin, J. Solid State Chem. 118 (1995) 74.
[13] E.R. Franke, H. Schaefer, Z. Naturforsch. 27B (1972) 1308.
[14] R.D. Sannon, C.T. Prewitt, Acta Crystallogr., Sect. B 25 (1969) 925.
[15] G. Savelsberg, H. Schaefer, Z. Naturforsch. 33B (1978) 370.
[16] Y.C. Wang, F.J. DiSalvo, J. Solid State Chem. 156 (2001) 44.
[17] P. Kubelka, F. Munk, Z. Tech. Phys. 12 (1931) 593.
[18] P. Kubelka, J. Opt. Soc. Am. 38 (1948) 448.
[19] R. Dalvern, J. Appl. Phys. 41 (1970) 5034.
[20] K. Ueda, H. Hosono, N. Hamada, J. Phys.: Condens. Matter 16 (2004) 5179–5186.